Thesis for the Degree of Master of Engineering

# Synthesis of Metal Nanoparticles in Diblock Copolymer Micelles and Their Surfaced-Enhanced Raman Scattering

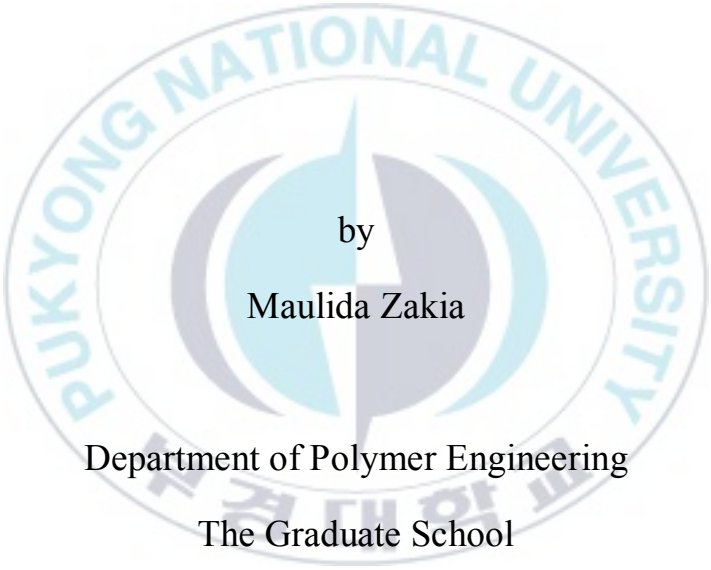


by

Maulida Zakia

Department of Polymer Engineering

The Graduate School

Pukyong National University


June 2017

# Synthesis of Metal Nanoparticles in Diblock Copolymer Micelles and Their Surfaced-Enhanced Raman Scattering

Advisor: Prof. Seong Il Yoo

by

Maulida Zakia

A thesis submitted in partial fulfillment of the requirements

for the degree of

Master of Engineering

in Department of Polymer Engineering, The Graduate School,

Pukyong National University

Busan, South Korea

June 2017

# Synthesis of Metal Nanoparticles in Diblock Copolymer Micelles and Their Surfaced-Enhanced Raman Scattering

A thesis

by

Maulida Zakia

Approved by:

Prof. Joo Hyun Kim

Prof. U Hyeok Choi

Prof. Seong Il Yoo

June 2017

**CONTENTS**

# LIST OF TABLES

# LIST OF FIGURES

# Synthesis of Metal Nanoparticles in Diblock Copolymer Micelles and Their Surfaced-Enhanced Raman Scattering

Maulida Zakia

Department of Polymer Engineering,

The Graduate School

Pukyong National University

## Abstract

Superstructures assembled from diblock copolymer micelles and metal nanoparticles (NPs) are continue to grow owing to their precise control of the NPs placement within the micelles. Moreover, the interaction between NPs also have the potential to reveal new properties different from single NPs. In this study, we assemble PS-PAA micelles containing Au nanoparticles in the core, which further develop as building block for the second-level assembling process. The cluster-like formation of Au NPs can be controlled by variation of temperature, solvent, and salt concentration. On the other hand, heterogeneous metal nanoparticles assemblies consisting of Au and Ag nanoparticles are also interesting because both component NPs exhibit localized surface plasmon resonance (LSPR) in visible region. By utilizing different domains in micellar structure, we arrange Au and Ag NPs in separate location to induce the plasmonic coupling. Here, the surface of Au NPs was modified by Raman active ligand, which was surrounded by Ag NPs in the assemblies. Notably, the SERS signal from heterogeneous metal assembly are dramatically increased in comparison to individual constituent NPs. To studied

further, we evaluated the SERS activity by controlling the physical dimension of Au NPs. This result demonstrate that superstructures micellar hybrid provides an interesting opportunity for SERS application.

# 이중 블록공중합체에 마이셀을 이용한 금속 나노입자 자기조립체 형성과 표면증강 라만산란 응용

## 요약

블록 공중 합체 마이셀 및 금속 나노 입자 (NP)에서 조립 된 구조체는 미셀의 NP 배치의 정확한 제어를 위해 계속해서 발전해 나가고 있다. 또한 NP 사이의 상호 작용은 하나의 NP와는 다른 새로운 특성을 나타낸다. 본 연구에서는 코어에 Au 나노 입자를 도입한 PS-PAA 미셀을 조립하였으며, 더 나아가 두단계 조립 단계를 발전시켰다. Au 나노입자의 클러스터 형태는 온도, 용매 및 소금 농도의 의해 조절 된다. 한편, Au 및 Ag 나노 입자로 구성된 이종 금속 나노 입자는 가시광선 영역에서 국소 표면 플라스 몬 공명 (LSPR)을 나타내기 때문에 관심 받고 있다 . 미셀 구조 중 다른 도메인을 이용하여, 본 연구에서는 Au와 Ag NPs를 분리된 위치에 배치하여 플라즈모닉 커플링을 유도하였다. 이때, Ag NP로 표면이 둘러싸인 Au NP는 라만 활성 리간드에 의해 배열 된다.주목해야 할 것은, 이종 금속 어셈블리에서 SERS 신호는 개별 구성 성분의

NP에 비해 극적으로 증가한다. 더 나아가, 본 연구에서는 Au NP의 물리적 크기를 제어하여 SERS 활성을 평가하였으며, 이러한 연구 결과는 미셀 하이브리드 구조의 SERS 분야에서 많은 응용 가능성을 보여준다.

# Chapter I. Introduction

## I-1. Metal Nanoparticles

Nanoparticles defined as particles of any shape with a size between 1 and 100 nm. Therefore nanoparticles possess distinctively different properties compared to those of bulk materials. They also strongly depend on the size and shape of the particles [1,2]. The ability to influence the properties of such nanostructures by controlling their geometry made this field very attractive and was one of the main reasons why the number of research projects focused around this topic was dramatically increased within the last decades [3-5].

### I-1.1 Localized Surface Plasmon Resonance

When a small spherical metal nanoparticle is irradiated by light, it produces a strong interaction between the incident electric field and the free conduction electrons of the metal NPs [6-11]. When the frequency of the free electron oscillation is the same as that of the incident light, constructive interference results in the strongest possible oscillation as well as localized field strength. This phenomenon is defined as the localized surface plasmon resonance (LSPR) and dominates the optical response of the nanostructure. The LSPR of metal NPs is strongly dependent on the dielectric constant of the metal and the surrounding material as well as the size and shape of the NPs [11]. Hence, it is possible to modify the LSPR of metal NPs simply by

synthesizing the preferred NP size and shape.

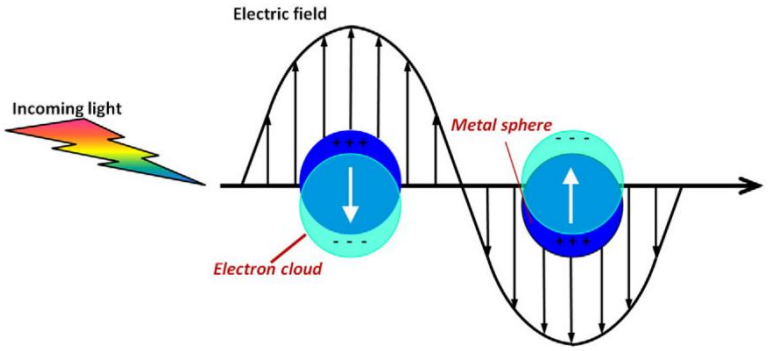


**Figure 1.** Schematic diagram of a localized surface plasmon resonance (LSPR) induced by an external electrical field.

## I-1.2 Plasmonics Coupling

When two or more NPs are in close vicinity, the localized particle plasmons of the individual NPs interact with each other via their optical near fields, creating coupled LSPR modes [11]. This is known as plasmonic coupling and results in new hybridized plasmon modes. As seen in Figure 2, the spectral position of coupled NPs depend strongly on the interparticle distance and configuration, showing large spectral shift with respect to the localized plasmons of the individual NPs and red-shift significantly when the distance between the particles is reduces. Utilization of plasmonic coupling is hence a powerful way to tune the plasmon frequency.

Plasmonic coupling between closely spaced metal nanostructures generates large near-field enhancement in the gap between the particles, usually called “hot spots”. These hot spots are especially interesting for SERS, where the large field strengths can be used to increase the Raman scattering signals from specific molecules placed inside the enhanced near-fields [12].

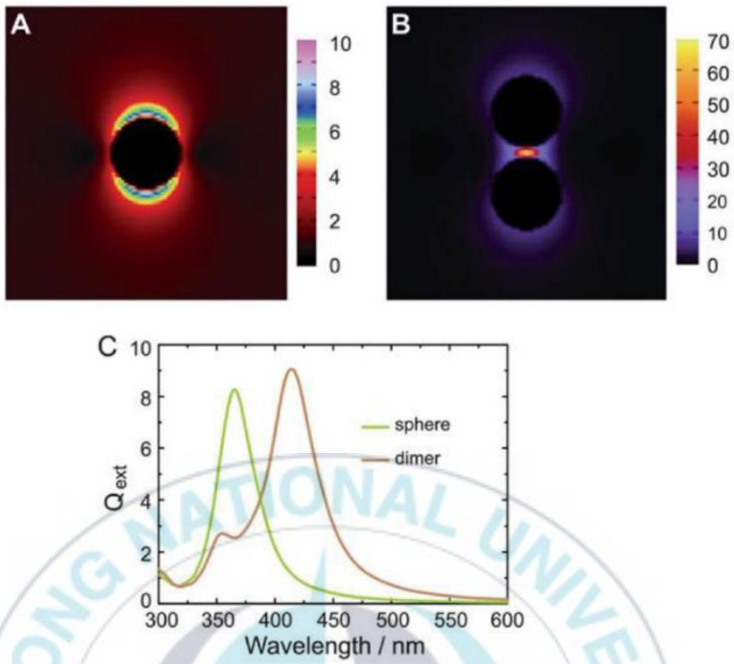


**Figure 2.** Plasmonic coupling (A, B) Near field enhancement distribution produced by a silver spherical NP with D = 25 nm and by a pair of spherical NPs of the same diameter separated by 5 nm, respectively. (C) Spectra of the single spherical NP and the NP pair shown in A and B [11].

## I-2. Surface-Enhanced Raman Scattering (SERS)

### I-2.1 Raman Scattering

In 1928, the Indian physicist C.V Raman discovered that when light was scattered from the molecules, scattering process results two types of scattered light, one of which had the same energy as the incident light and the second one, small fraction of scattered light had different energy of when the molecules were responsible for the scattering [13]. When molecules are irradiated by electromagnetic radiation of a single frequency, the molecule can be excited into one of the infinite virtual states. When the molecule return to the ground state, a photon may be reemitted. If the photon emitted is of the same frequency, the scattering is termed elastic and this phenomenon is called Rayleigh scattering (Figure 3). In contrast, Raman scattering is inelastic because the photon reemitted has a different frequency, described as Stokes scattering if the new photon is at a lower frequency than the original and anti-Stokes scattering if it is at a higher frequency than the original. Usually, Stokes scattering is followed in Raman Spectroscopy since anti-Stokes scattering is less intense. The energy difference between the incident and scattered light is called Raman shift and is calculated in wavenumbers through equation (1), in which ΔE is Raman shift in wavenumbers, $\lambda_{incident}$ is the wavelength of incident light in nm and $\lambda_{scattered}$ is the wavelength of scattered light in nm.

$$\Delta E = \frac{1}{\lambda_{incident}} - \frac{1}{\lambda_{scattered}}$$

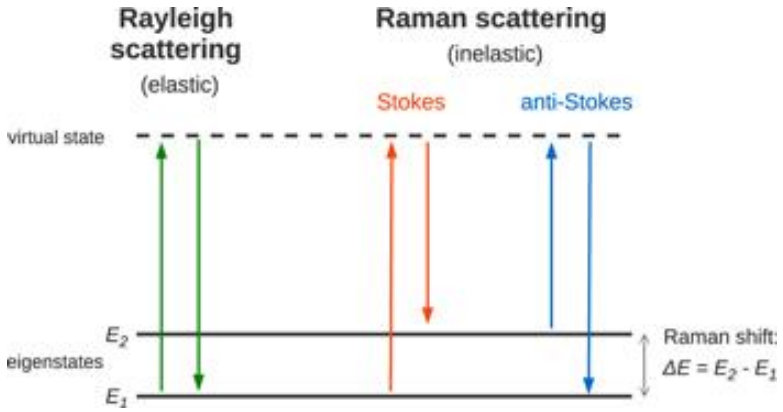


**Figure 3.** Schematic of the Rayleigh and Raman scattering processes.

## I-2.2 Surface-Enhanced Raman Scattering (SERS)

The enhanced Raman signal of pyridine adsorbed on roughened electrochemical silver electrode, observed by Fleischmann et. Al in 1974 [14], is considered to be the first observation of the SERS effect. Surface enhanced Raman spectroscopy (SERS) is a variant of Raman spectroscopy that exploits nanoscale phenomena. The discovery of SERS has opened a promising way to overcome the traditionally low sensitivity problem in Raman spectroscopy [15]. Raman signal are normally very weak and can only be used for bulk samples or concentrated solutions. SERS is all about amplifying Raman signals, almost exclusively from molecules, by several orders of magnitude. Metal NPs (typically gold and silver) could tremendously enhance the Raman cross-section of the sample molecules that are in a certain proximity of the metal surface due to the large electromagnetic field induced by LSPR [16].

SERS enhancements are mainly attributed to the electromagnetic (EM) and chemical (CE) effects [17]. In theory, EM enhancement is caused by the surface plasmon resonance generated on the metal surface while CE involves changes to the adsorbate electronic states due to chemisorption of the analyte. There is still a degree of uncertainty regarding the level of enhancement from each mechanism. This uncertainty comes from a difficulty of the SERS experiments since samples are random in nature. It is difficult to quantify where the SERS signal comes from.

### I-2.3 Electromagnetic Enhancement

According to the EM model, the increase in the Raman intensity is caused by extremely high local electromagnetic fields that arise from localized surface plasmon resonance (LSPR), where it is called “hot-spots”. Typical metals that support surface plasmons are silver, gold and copper. Generally, silver generates more surface plasmon than other metals due to its large negativity of dielectric constant. Resonance occurs when an electric field (laser light) at a certain incident wavelength excites the localized surface plasmons in strong light scattering, resulting in the appearance of intense surface plasmon absorption bands and an enhancement of the local electromagnetic fields. The frequency and intensity of the surface plasmon absorption bands depend on the type of metal, nanostructure size, size distribution, and shape, as well as the environments which surround them. Generally, electromagnetic enhancement relies on Raman-active molecules being confined within these electromagnetic fields.

### I-2.4 Chemical Enhancement

The EM mechanism can not account for all the enhancement phenomena observed in SERS experiments [15,17]. The chemical enhancement mechanism is due to a charge transfer between the metal and the adsorbed molecules. According to the chemical theories, the polarizability of the molecule-metal system should be studied under conditions of adsorption, since Raman

scattering from an isolated molecule is a result of the modulation of the electronic polarizability of the molecule, consequently, new excited states will appear due to the possibility if charge transfer and local changes in the electron charge density near the surface because of chemical bonding or tunneling of electrons from the metal to the molecule. Chemical mechanism exist when the distance between the molecule and the metal is in the order of the atomic size. The chemical nature of the molecules and the adsorption sites of the surface are the major factors determining Raman scattering enhancement, the observed SERS spectra can differ significantly from the corresponding Raman spectra if non-adsorbed molecules.

### I-2.5 Plasmonic Nanostructures for SERS Application

Surface-enhanced Raman spectroscopy (SERS) has become a useful analytical tool for improvement of chemical analysis and biology sensors. Raman enhancement occurs when the molecules attach to the surface of metal NPs. There are “hot spots” existing at the surface owing to the localized surface plasmon resonance. Design of maximum hot spots of metal NPs is an important principle for SERS design. Recently, there are a lot of designs of SERS substrates that have been reported through controlling the shape and size of metal nanostructures [18-24]. The size and shape of plasmonic nanostructures are two big factors strongly influencing the enhancement.

## I-3. Self-Assembly of Block Copolymer

Block copolymers are a unique class of materials well-known for their ability to self-assemble into well-ordered nanometer scale microdomains. In a block copolymer, two or more chemically incompatible polymer chains are covalently linked and this linkage prevents macrophase separation [25,27]. However, due to the unfavorable interactions between the different blocks, phase separation still occurs on nanometer scale and this process is called microphase separation. The theory of BCs self-assembly is well-developed and successfully predicts the phase diagram of the equilibrium morphology of BCs, as shown in Figure 4. The self-assembly process of block copolymers is determined by three experimentally controllable factors : the degree of polymerization ($N$), the volume fraction of component blocks ($f$), and the Flory-Huggins interaction parameter ($\chi$). By manipulating these factors various morphologies (spheres, cylinders, gyroid, lamellae) have been revealed [26-27].

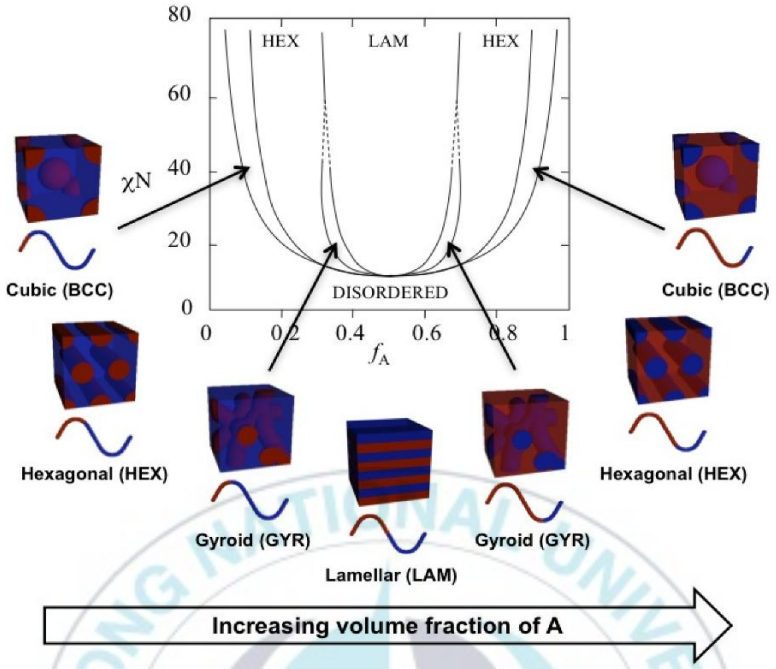


**Figure 4.** Phase diagram of a diblock copolymer, calculated using self-consistent mean field theory. Regions of stability of disordered (dis), lamellar (lam), gyroid (gyr), hexagonal (hex) and body-centered cubic (BCC) phases are indicated. Adapted from reference [26-27].

## I-3.1 Block Copolymer Micelles

Block copolymers self-assemble to form micelles when dispersed in a selective solvent for one of the blocks. Micellization is an enthalphic process of reduction of free-energy. The unfavorable enthalphic interaction between the hydrophobic block and the solvent are avoided with the formation of micelles. The soluble block will be oriented towards the solvent medium and become the ‘corona’ of the micelle forms, whereas the insoluble part will be shielded from the solvent in the ‘core’ of the structure. Moreover, different sizes of blocks lead to specific architectures of micelles. If the soluble block is larger than the insoluble one, the micelles formed consist of a small core and a very large corona, and are thus called ‘star micelles’. By contrast, micelles having a large insoluble segment with a short soluble corona are referred to as ‘crew-cut micelles’.

Micelle formation is generally observed above a critical micelle concentration (CMC) and critical micelle temperature (CMT), which can be defined as the concentration and temperature at which micelles become detectable. Below CMC and CMT, self-assembly will not occur, and the BCs will behave in the solution as a unimer. Due to their ability to self-assemble into various nanoscaled structures, BCs have been widely used as building blocks that can further assemble into complex hierarchical structures by chemically or physically binding these assemblies together [28-35].

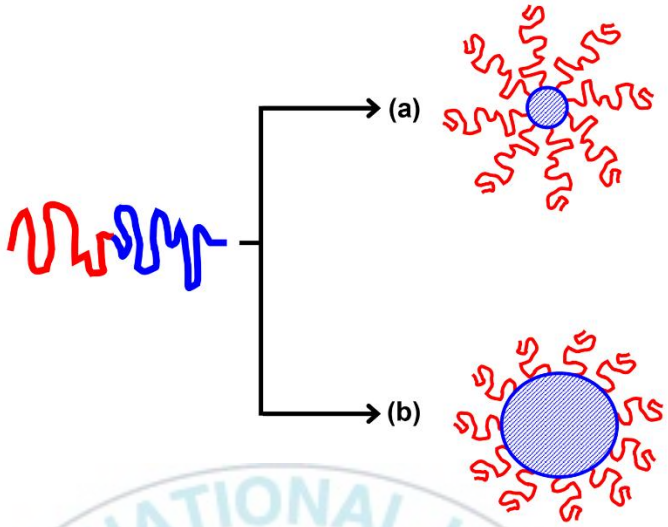


**Figure 5.** Schematic representation of : (a) star micelle, (b) crew-cut micelle

# Chapter II. Clustered Assembly of Au Nanoparticles from Spherical Diblock Copolymer Micelles Encapsulating Au Nanoparticle [36]

## II-1. Introduction

In a selective solvent, diblock copolymers self-associate into micelles consisting of solvated coronas and insoluble cores [37-39]. Core and corona structures of micelles have been widely utilized for the stabilization and solubilization of inorganic nanoparticles (NPs) which are otherwise insoluble a given solvent [24,29-31,34,40-52]. For instance, Taton's group utilized PS−PAA diblock copolymers to encapsulate hydrophobic Au NPs into the PS core of micelles in an aqueous solution [29,42]. In their report, Au NPs having diameter smaller than 10 nm primarily behave as solute. Therefore, those NPs can be concurrently encapsulated into the same core of micelles, resulting in multiple NP encapsulation [42]. On the other hands, when large Au NPs (diameter > 10 nm) have been employed, single NP was mostly placed in the center of micelles because the large NPs behave as surface, onto which polymer chains can be adsorbed [42]. After their pioneering reports, many research groups published interesting encapsulating methods of metal, semiconductor, and oxide NPs into

micellar structure with controllable arrangement [34,43-52]. Here, this kind of NP assembly is quite attractive because the specific arrangement of inorganic NPs with the micellar structure can reveal interesting opportunities in photonic, sensing, catalytic, and biological applications [24,34,40,41,45-47].

In the micellar hybrids, the distribution or arrangement of NPs could be regulated by a number of methods. For instance, the local position of NPs can be regulated by the micellar structure without specific structural transformation [29,34,42-44]. In this approach, the surface chemistry of NPs is often modified by various ligands to engineer specific interactions with constituent blocks of copolymers, which can allow a direct positioning of NPs in the core, corona, and interfaces of micelles [30,43,44]. In another set of experiments, specific NP arrangement is pre-determined in a solution state and then fixed by micelles [31,48]. For instance, it has been reported that many inorganic NPs can be re-arranged into one-dimensional chains. In this regard, Chen et al studied salt-induced linear assembly of Au NPs in DMF solution [31]. In particular, they found that the growth of NP chain can be terminated by the addition of PS−PAA copolymers and water. Since water is a selective solvent for PS block, PS−PAA copolymers spontaneously formed a cylindrical micelle which surrounds the linear assembly of Au NPs. Alternatively, Liz-Marzán et al. utilized hydrophobic interaction to produce three-dimensional cluster-like NP assembly [48]. In their study, they first prepared stable dispersion of polystyrene−coated Au NPs (PS−Au NPs) in THF solution. Subsequently, an aggregation of PS−Au NPs has been initiated upon the addition of water, i.e., a poor solvent for polystyrene. They discussed that the

growth of NP aggregation increases with incubation time but can be quenched by the addition of PS−PAA copolymers, resulting in the sequestration of NP clusters inside the PS−PAA micelles.

Interestingly, it has been recently reported that micelles containing NPs can be further utilized as a building block for the second-level assembling process; this can produce multiple colloidal superstructures with more variability and complexity in the NP arrangements [49-52]. For instance, Chen et al. reported that Au NP encapsulated by PS-PAA micelles (Au@PS−PAA micelle) in DMF/water solvent could behave quite analogous to monomers, and can be polymerized into long chains by the addition of salt. They discussed that the attachment of free Au@PS−PAA micelle to the end of growing chain is more energetically favorable, resulting in the formation of cylindrical NP assembly inside micelles [49]. In attempt to produce more complex structure, Mottitt et al. prepared micelle-encapsulated NPs, at which the outer corona is composed of both hydrophobic and hydrophilic chains [52]. By adding polar solvent that can only dissolve the hydrophilic blocks, the micellar structures could be re-organized into janus-type conformation, which is subject to form more complex superstructures. In fact, this kind of methods is quite attractive because not only the arrangement of NPs can be in-situ controlled by the structural change of block copolymer micelles, but also the resulting NP patterns can exhibit collective properties beyond the function of individual constituent NPs. However, there is still limited number of publications toward this research direction.

In this perspective, we report a feasible approach to produce cluster-like assemblies of Au NPs by structural re-organization of spherical Au@PS−PAA micelles. Here, we first prepared Au@PS−PAA micelles in an aqueous solution, which were then re-dispersed into a mixed solvent of $H_2O$/DMF. By adding HCl into the solution of Au@PS−PAA micelles, the overall equilibrium condition for given Au@PS−PAA micelles has been altered to initiate clustering of Au NPs in the core of micelles. The resulting clustered NPs in the micellar assembly exhibited red-shifted UV-Vis spectrum, which was strongly correlated with the collective interaction among NPs in the core of micelle.

## II-2. Experimental Section

### II-2.1. Material

Gold (III) chloride trihydrate (HAuCl4, 99.9%), 2-naphtalenthiol (99%), sodium citrate tribasic dehydrate (99%), N,N-Dimethylformamide anhydrous (DMF, 99.8%) were purchased from Sigma-Aldrich and were used as received. Hydrochloric Acid (HCl, 35%) was obtained from Junsei. Polystyrene-*block*-poly(acrylic acid), PS−PAA, diblock copolymer was obtained from ATRP Solution Inc. The degree of polymerization of PS and PAA in the PS-PAA copolymers was 198 and 55, respectively, with a polydispersity index of 1.12. Dialysis membrane having molecular weight cut off of 3.5 KDa (Spectra/ Por 7) was purchased from Spectrum Laboratories Inc.

### II-2.2. Procedure

#### II-2.2.1. Synthesis of Gold Nanoparticles

Au NPs were synthesized by citrate reduction method. Briefly, 500 mL aqueous solution of HAuCl4·3H2O (0.5 mM) was heated until boiling, and 25 mL of sodium citrate solution (0.5 g in 25 mL) was added to the boiling solution. The mixture was further boiled for 15 min with vigorous stirring and then cooled to room temperature.

#### II-2.2.2. Surface Modification of Gold Nanoparticles

The surfaces of Au NPs were modified by ligand exchange reaction using 2-naphthalenethiol, a hydrophobic ligand. To this end, the as-prepared Au NPs were centrifuged (9000 rpm, 40 min) and then redispersed into N,N-dimethylformamide (DMF). Subsequently, 2-naphthalenethiol (180 μL, 1.0 wt % in DMF) was added to the purified Au NP solution (18 mL), which was further incubated at 60 °C for 1 h to complete surface modification.

#### II-2.2.3. Encapsulation of Au NPs inside PS−PAA core

PS−PAA micelles containing Au NPs in the core were prepared according to a literature method with slight modification. First, independently prepared DMF solutions of 2-naphthalenethiol- modified Au NPs (4.5 mL) and PS−PAA copolymers (4.5 mL, 0.1 wt % in DMF) were mixed together. Second, deionized water (2 mL) was added to the solution mixture such that the $H_2O$ concentration in the total solution becomes ∼18 vol %. Third, the mixture was heated to 110 °C for 2 h and then slowly

cooled to room temperature. Next, the solution was dialyzed against $H_2O$ to remove DMF and residual reagents. In a typical dialysis process, the mixture solution (30 mL) was added to a dialysis membrane. After clamping, the dialysis membrane was placed in a large beaker filled with $H_2O$, which was then gently stirred at room temperature. Deionized water was exchanged for each 12 h at least two times.

### II-2.2.4. Synthesis of Cluster-like Au NPs

In this set of experiment, first, Au@PS−PAA micelles in an aqueous solution (2.0 mL) have been precipitated at the bottom of Eppendorf tube by centrifugation (9000 rpm, 90 min). Subsequently, the supernatant was cautiously removed by micro-pipette and the volume of the resulting precipitates was adjusted as approximately 50 mL. Next, the precipitates were transferred to a glass vial, onto which a mixed solvent consisting of deionized $H_2O$ and N,N-dimethylformamide (DMF) (typically, 5% v/v of $H_2O$) was added until the absorbance of Au NPs at 535 nm became 0.5 when measured by UV-Vis spectroscope with a cuvette having a path length of 1.0 cm. Finally, an aqueous solution of HCl (typically 10 mM) was further added to the solution, and the resulting mixture was incubated without stirring at room temperature and then transferred to oil bath at 60 °C. After a certain period of time, the solution was dipped in the ice-cold water to quench the assembling process.

### II-2.3. Measurement

UV−Vis absorbance data were recorded on a JASCO V-670 spectrophotometer.

Dynamic light scattering (DLS) and zeta-potential measurements were performed on a Zetasizer Nano ZS-90 (Malvern Instruments). Transmission electron microscopy (TEM) images were recorded on a Hitachi H-7500 instrument operating at 80 kV.

## II-3. Results and Discussion

### II-3.1. Encapsulation of Au NP in Diblock Copolymer Micelles

In an aqueous solution, PS−PAA diblock copolymers spontaneously aggregate into micelles consisting of PS cores and PAA coronas [30,37,40,41,53,54]. Initially, we encapsulated 2-naphthalenethiol modified Au NPs in the PS core of PS−PAA micelles as described in the experimental section. In this step, even though the hydrophobic ligand (2-naphthalenethiol) does not have compatibility with PS block, 2-naphthalenethiol modified Au NPs can be inserted into PS core of micelles to avoid unfavorable contact with $H_2O$. As shown in the TEM image of Figure 6a, the as-prepared Au NPs have spherical shape and an average diameter was evaluated as 12 nm. After the encapsulating process (Figure 6b), the surface of Au NPs was uniformly coated by polymer shell that can be clearly distinguishable in the TEM images by the contrast difference with Au NP in the core. Noticeably, single NP is placed at the center of each micelle because Au NPs larger than 10 nm can primarily behaves as surface, onto which PS block of PS−PAA copolymers can be adsorbed during micellization [42]. In parallel, the extinction maxima of Au NPs before and after encapsulation process were found at 518 nm (dashed line in Figure 6c) and 535 nm

(solid line in Figure 6c), respectively. Since extinction position of metal NPs is proportional to the refractive index of local environment, the red-shifted UV-Vis spectrum after the encapsulation step further confirmed the formation of Au@PS−PAA micelles (Note, the refractive indices are 1.59 for PS block and 1.33 for water, respectively)

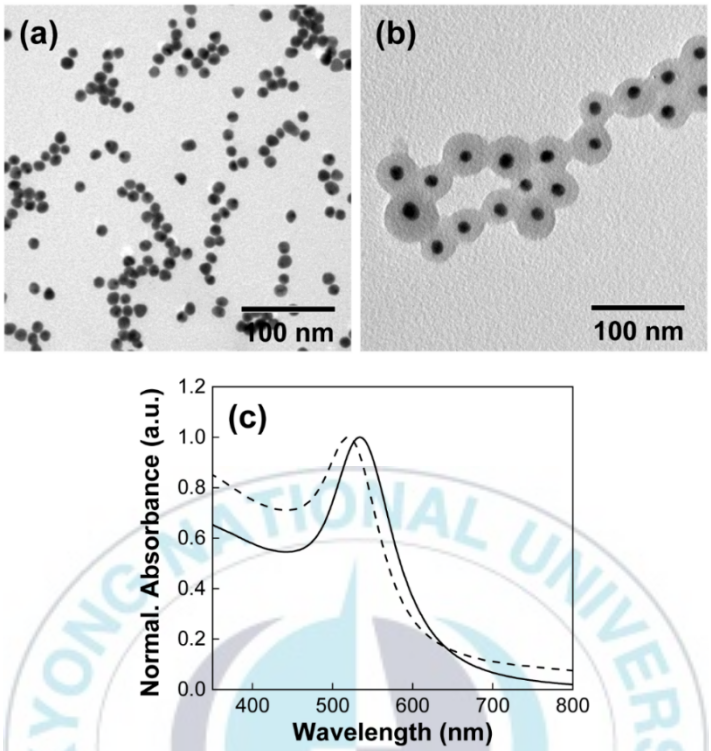


**Figure 6.** (a, b) TEM images of (a) Au NPs and (b) Au@PS–PAA micelles with Au NP in the core. (c) UV-Vis spectra of pure Au NPs (dashed line) and PS–PAA micelles with the Au NP in the core (solid line).

### II-3.2. Clustered Assembly of Au Nanoparticles

Next, we turned our attention on the morphological transition of the Au@PS–PAA micelles. At the beginning, it would be instructive to note that the micellization is mainly driven by the unfavorable contact between the core-forming block and solvent. In this regard, an increase in the micellar size is thermodynamically favorable because the total interfacial energy between the core and solvent can be decreased with the core size [30,53,54]. However, an increase in the micellar core involves the stretching of core-forming blocks as well as the strengthened repulsion among corona-forming blocks, which has an adverse effect on the stabilization [30,53,54]. Therefore, these three factors usually compete with each other to determine the equilibrium morphology of block copolymer micelles. In this regard, we added HCl (aq) to the micellar solution in attempt to adjust the degree of protonation of carboxylic acid in corona-forming PAA block. Note, this process reduces the strength of repulsion among negatively-charged corona blocks, which could be counterbalanced by additional increase in the core; hence, the overall equilibrium condition for given micelles can be simultaneously adjusted to induce morphological transition. However, it must be noted that a structural change of Au@PS–PAA micelles would not be allowed by simple addition of HCl (aq) because the Au@PS–PAA micelles in Figure 6 are kinetically frozen state by the glassy PS cores in water. In this reason, Au@PS–PAA micelles in an aqueous solution were first precipitated by centrifugation and then re-dispersed into a mixed solvent of $H_2O$/DMF. Here, DMF is a good solvent for both blocks, and therefore core-forming PS block can be substantially swollen by the DMF

and attain substantial chain mobility in a solution state. It would be worthwhile to note that our method is quite analogous to those reported from literature, at which morphological transformation of ionic micelles (with and without NPs) has been studied by the addition of salt or change of pH [51,53,54].

In the first set of experiment, we re-dispersed Au@PS–PAA micelles in 4 mL of $H_2O$/DMF solvent (5% v/v $H_2O$), onto which 50 μL of HCl (10 mM) was further added. Subsequently, in attempt to get the overall structural information, UV-Vis spectra of the solution were monitored in different periods of time as shown in Figure 7a. When Au@PS–PAA micelles were initially re-dispersed in $H_2O$/DMF solvent, the extinction peak of Au NPs was basically maintained as depicted in black line (Figure 7a), which can be ascribed to the localized surface plasmon resonance (LSPR) of isolated Au NPs. Even after the addition of HCl (aq), the UV-Vis spectrum remained nearly the same (not shown); this might suggest that no significant structural changes of micelles had been occurred upon the protonation of carboxylic acid of PAA corona, which appears to contradict the initial anticipation. As a matter of fact, it turns out that the morphological change of Au@PS–PAA micelles was very slow at room temperature. For instance, after 4 days of incubation at room temperature, a structural transformation starts to be appeared as shown in Figure 7b, in which two or three NPs are merged together in the same core of micelles.

In this reason, we elevated the temperature of the solution up to 60$^{o}$C to speed up the overall kinetics. In the elevated temperature, the morphological changes was

dramatically accelerated. Just after 3 min incubation, pink color of the original solution was slightly changed to violet, which had been accompanied with the red-shifted extinction peak of Au NPs to ~547 nm (blue line in Figure 7a). In general, when metal NPs are placed in a close proximity with each other, LSPR of adjacent NPs couples together, resulting in a peak shift to a longer wavelength direction [48,50,55,56]. In this regard, the red-shifted plasmonic peak of Au NPs with a color change in the solution could be a strong indication of the structural change of Au@PS–PAA micelles because the direct plasmonic coupling of Au NPs was initially inhibited by the micellar coating on each NP. As confirmed from Figure 7c, Au@PS–PAA micelles were transformed into larger micellar assemblies with clustered NPs in the center. In the TEM image, Au NPs are closely positioned with each other, but their direct contact appears to be avoided; this should be responsible for the plamonic coupling in the UV-Vis spectrum. Interestingly, after the initial formation of clustered NP assembly within 3 min, the growth of micellar NP assemblies only marginally increased with the incubation time, as shown in Figure 7d – 7f. This is further supported by the limited spectral shift in UV-Vis spectra of Figure 7a with incubation time. Note, a significant increase in the number of NPs in the assemblies entails additional plamonic coupling, which has to be detected by more extensive red-shifts in UV-Vis spectrum.

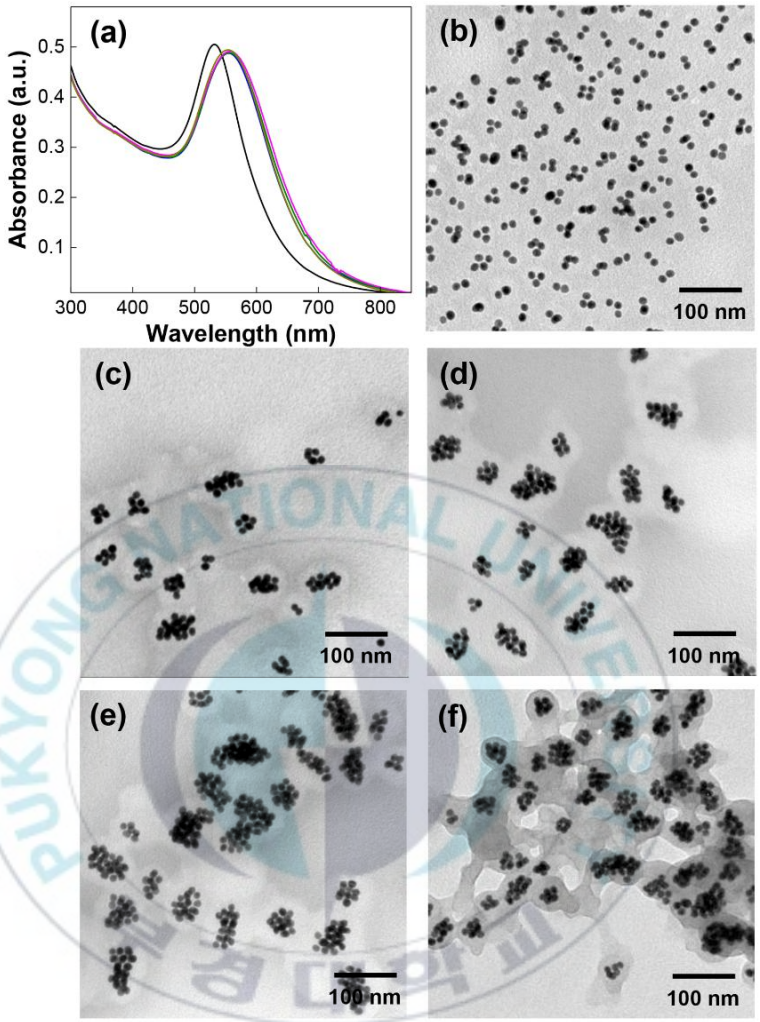


**Figure 7.** (a) UV-Vis spectra of Au@PS–PAA micelles after being re-dispersed in $H_2O$/DMF solvent (black), heated for 3 min (blue), 10 min (green), 30 min (pink), and 60 min (dark yellow). The heating was followed by the addition of HCl (aq). (b – f) TEM images of clustered NPs in micelles corresponding to different incubation condition: (b) room temperature for 4 days; (c – f) after being heated for 3 min (d), 10 min (d), 30 min (e), and 60 min (f).

### II-3.3. Effects of Temperature on the Growth of Clustered Assembly of Au Nanoparticles

The experimental observation in Figure 7 further suggested that the kinetics of clustering formation could be strongly affected by temperature. In this regard, we further studied the effect of temperature on the growth of micellar assemblies. In particular, considering the rapid rise in the number of NPs at the early stage of incubation, we focused on the TEM observation on the assembled structures after 10 min of incubation. As shown in Figure 8, it is clear that the number of NPs in the micellar assemblies gradually increases with increasing temperature from room temperature (Figure 8a), 30°C (Figure 8b) and to 50°C (Figure 8c), respectively, which clearly demonstrated the temperature effect on accelerating the assembling kinetics.

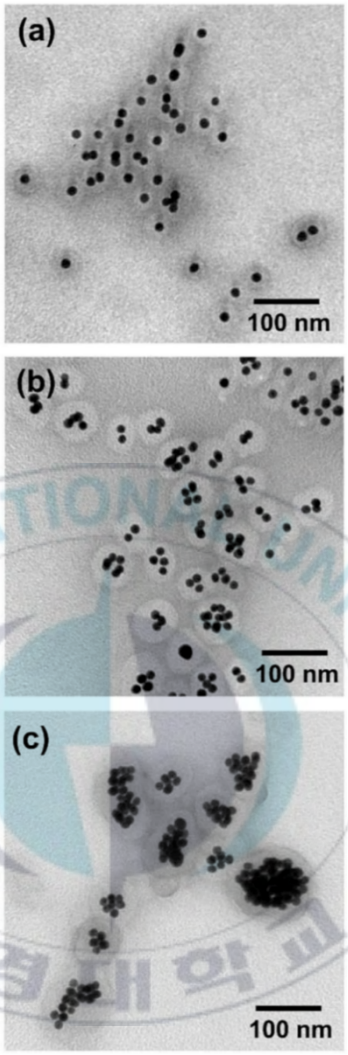


.5

**Figure 8.** TEM images of clustered NPs in micelles after being incubated for 10 min at different temperature: (a) room temperature, (b) 30°C, (c) 50°C.

### II-3.4. The Growth Pattern of Clustered Assembly of Au Nanoparticles

To better analyze the growth of micellar NP assemblies with incubation time, we evaluated the number of NPs in each micellar assemblies as well as the thickness of polymer coating surrounding the NPs from the TEM images of Figure 7. On examining the results, it would be worthwhile to note that the superstructures of micellar NP assemblies showed a certain distribution at each preparation time. Hence, the statistical results in Figure 9, which have been collected from four independent TEM measurements, contain relatively broad distribution. Nevertheless, one can clearly monitor the growth pattern of the assemblies with incubation time. For instance, after 3 min of incubation, the average number of NPs in the micellar assembly was determined as 6 with a standard deviation of 3.4. This value was slightly increased with incubation time as to 9 ± 5.1 (for 10 min), 12 ± 6.7 (for 30 min), and 14 ± 8.1 (for 60 min), respectively, as shown in Figure 9a. However, further increase in the incubation time (up to 24 hr) did not noticeably raise the NP numbers. Instead, the structure of micellar assemblies became more or less deteriorated, which restricted further analysis. At the same time course, the change of thickness of polymer coating surrounding the clustered NPs has been analyzed. Initially, the thickness of polymer coating on Au@PS-PAA micelles before assembling process was determined as 11.5 ± 1.0 nm from Figure 6b. This value was increased to 17.3 ± 3.4 nm just after 3 min of incubation, and then maintained without noticeable changes, as shown in Figure 9b.

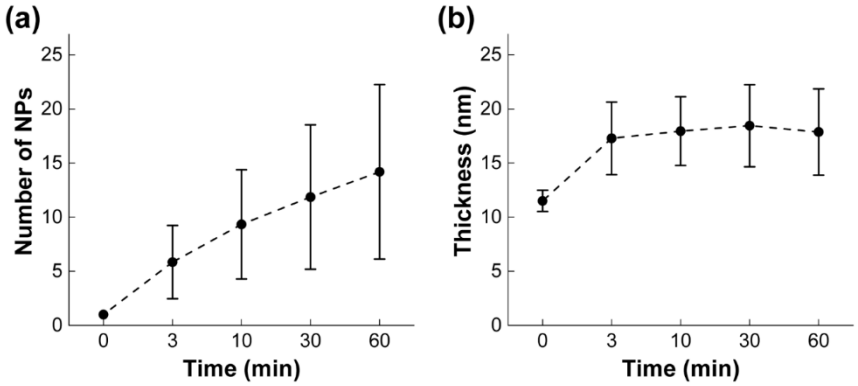


**Figure 9.** Changes of the number of NPs in the center of assemblies (a) and the thickness of polymer coating on the NPs (b) with incubation time. The results were collected and then averaged from four independent measurements.

The formation of clustered NP assemblies from Au@PS–PAA micelles would be understood as follows. Initially, the addition of HCl (aq) to the micellar solution reduces the electrical double layer repulsion among Au@PS–PAA micelles by protonating carboxylic acids in PAA block. This in turn increases possible collisions among Au@PS–PAA micelles. At the same time, the protonated PAA block with reduced electrostatic repulsion could induce the increase in the core diameter as discussed earlier [54]. Therefore, upon collision, PS–PAA copolymers tend to re-organize into more large micelles, which would be assisted by the swollen PS (as well as PAA) blocks in the mixed solvent. Along with the chain re-organization, 2-naphthalenethiol modified Au NPs tend to be phase-separated from PS blocks owing to their incompatibility, and therefore, they are subject to form clustered NPs in the center of micellar assemblies. The limited growth of NP assemblies in Figure 9 could be understood from the view point of polymer adsorption on the curved surface [42,57,58]. Note, the inclusion of many NPs in the same center of micelles alternatively decrease the surface curvature, which could increase inter-chain repulsions among tethered polymer chains. Hence, in order to alleviate the repulsion, the polymer chains tend to increase the end-to-end distance, resulting in the increased thickness of polymer layers [42,57,58]. Therefore, the more inclusion of NPs must entail further increase in the thickness of polymer coating, which would result in the enlarged entropic penalty by chain stretching of copolymers beyond the enthalpic gain by the protonation of PAA blocks. As a result, the growth of micellar NP assemblies would be terminated at the early stage of incubation without further

increasing NP numbers and the thickness of polymer coating, as discussed in Figure 7 and 9.

In this regard, the adjustment of experimental parameters such as the amount of $H_2O$ in the mixed solvent and the concentration of HCl (aq) did not produce larger assemblies having increased number of NPs. Rather, these control induced either inhibited or uncontrolled growth of the assemblies. For instance, we prepared the micellar NP assemblies with the same preparation method but changed water content in mixed solvent. In this experimental set-up, we re-dispersed Au@PS–PAA micelles into $H_2O$/DMF solvent having a reduced $H_2O$ (3.0 % v/v) to intentionally enhance the chain mobility of PS–PAA copolymers. Under this condition, TEM images showed comparable clustered NP assemblies in Figure 10b. However, UV-Vis spectrum (Figure 10a) exhibited red shift in the LSPR peak in a greater degree, indicating more extensive plasmonic coupling. On the other hand, when the water content was increased to 10.0 % v/v $H_2O$ in the mixed solvent, both UV-Vis spectrum (Figure 10c) and TEM image (10d) were not much altered in comparison with pure Au@PS–PAA micelle. Indeed, this observation can be ascribed to the restricted chain mobility in the high water content, which inhibited the re-organization of Au@PS–PAA micelles. In the next experiment, we increased the concentration of HCl (aq) from 0.01 M to 0.1 M under the same condition. Here, it can be anticipated that the greater protonation of PAA block would lead to more frequent collisions and reduced repulsion among the PAA blocks in the corona region, which could provide more favorable condition for the structural transformation. In this case, we observed

extensive red shift in UV-Vis spectrum (Figure 10e). However, the assembled structures mainly exhibited uncontrolled agglomeration of NPs (Figure 10f), which supports the aforementioned discussion.

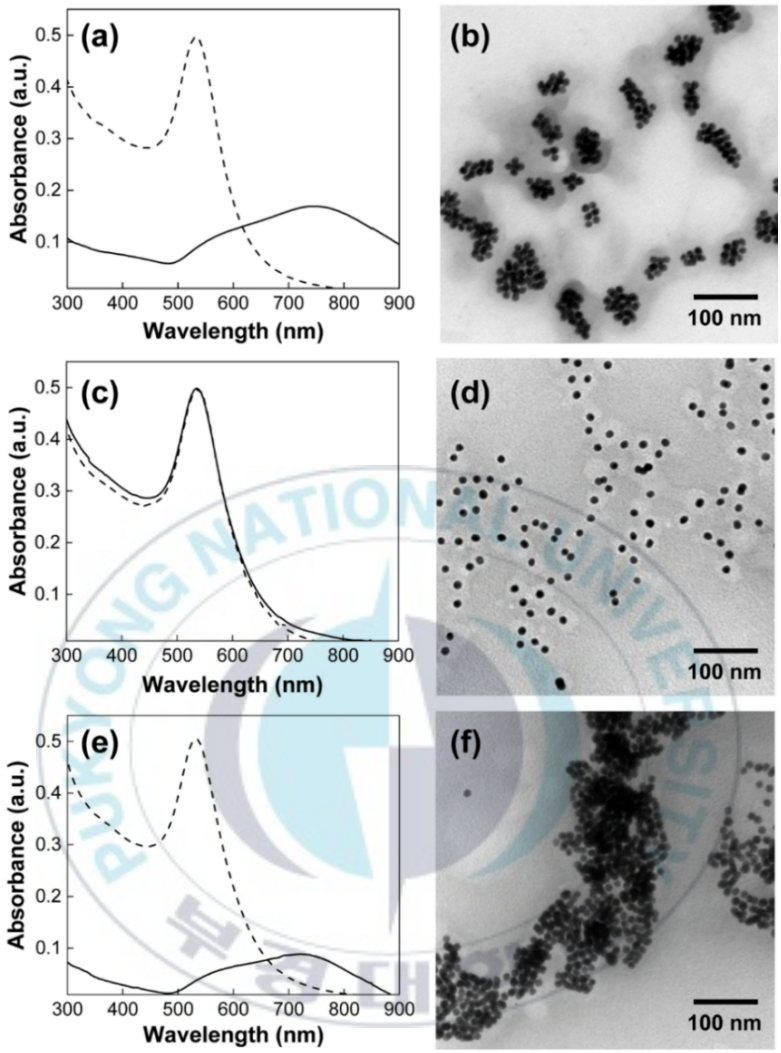


**Figure 10.** UV-Vis spectra and TEM images at different conditions: (a, b) HCl = 0.01 M, $H_2O$/DMF = 3.0 %; (c, d) HCl = 0.01 M, $H_2O$/DMF = 10.0 %; (e, f) HCl = 0.1 M, $H_2O$/DMF = 5.0 %. In UV-Vis spectra were collected after re-dispersing Au@PS–PAA micelles in $H_2O$/DMF solvent (dashed line), and heating for 60 min (solid line).

At last, it would be also interesting to compare the results in Figure 7 – 10 with the ones previous reported. In ref [51], Chen et al. reported a chain-growth polymerization mode of Au@PS–PAA micelles in acidic condition, at which a few active monomeric Au@PS–PAA micelle merged and transformed to long chains, while most of the monomeric micelles remains intact. Their chain-growth polymerization mode of Au@PS–PAA micelles appears to be controlled by kinetic reason, while thermodynamics also plays an important role. In particular, the attachment of monomeric Au@PS–PAA micelles was only allowed to the end of a growing chain by the reduced electrostatic repulsion at the highly curved chain end. Since the long chains only constituted a small population in the solution, they could not monitor the assembling behavior by UV-Vis spectroscope. On the other hand, the transformation of Au@PS–PAA micelles into clustered NP assembly in this study could be directly monitored by UV-Vis spectrum. Also, no individual Au@PS–PAA micelles were present in the TEM observation after the assembling process. This difference would be probably correlated with the small water content (typically 5%) in our condition, compared to that of Chen′s report (as high as 30%). Owing to the enhanced chain mobility by the small water content, re-organization of Au@PS–PAA micelles into spherical assemblies would be preferred at each successive collisions (Figure 7), which is quite different to the maintained cylindrical shape in ref [51]. As a result, the kinetic aspects on the end-on growth, which is only important to cylindrical assemblies, would not be crucial, but isotropic collision among micelles could mainly contribute to the morphological evolution.

Overall, this result clearly demonstrates that Au@PS-PAA micelles can be utilized as a building block for the second-level assembling process in creating colloidal superstructures. In this regard, it would be also worthwhile to note that step-wise assembling methods have been applied to thin film of block copolymers [59-60]. For instance, we reported bimodal assemblies of two different-sized spherical micelles by successive coating process [59]. In the study, a mono-layer film of large micelles having hexagonal order was initially fabricated as a pre-defined pattern, onto which small micelles were additionally deposited to form hierarchical nanostructures. While the experimental methods are different in each case, one may appreciate and compare the usefulness of step-wise assembling techniques in solution and thin film states for producing more complex and variable superstructures.

## II-4. Conclusion

In this study, we investigate a simple method to prepare clustered assemblies of Au NPs, which has been achieved by second-level assembling process of Au@PS−PAA micelles. The addition of HCl to the solution of Au@PS−PAA micelles protonated the carboxylic acid in PAA corona, which subsequently affected not only the equilibrium condition of given micellar structures but also the effective collision among Au@PS−PAA micelles. As a result, individual Au@PS−PAA micelles could be merged together to form more large micelles with inclusion of multiple NPs in the core. However, the gradual growth of the assembled structure was inhibited presumably by the entropic penalty associated with PS stretching. Considering that

the assembling process has been accompanied with red shifts in plasmonic peak of Au NPs, a relevant future work can be suggested as a systematic control on the diameter of Au NPs, which could reveal interesting properties of clustered NP assemblies from the view point of plasmonic coupling. In addition, the prospects of this result could be also assessed from the plasmonic coupling of given metal NPs in the assembled structure. For instance, metal NPs have been well known to enhance Raman signal of given analytes attached on their surface. Since this effect, known as surface-enhanced Raman scattering (SERS), could be dramatically enhanced at the gap region between adjacent metal NPs, the clustered NPs with plamonic coupling in the cores could provide gap plasmon to enhance SERS signals and therefore find opportunities in sensing applications.

* *This part of thesis has been published at Journal of Applied Polymer Science and resemble the accepted versions of reviewed journal with minor modifications and collaborate with Kim Jang Hwan.*

# Chapter III. Heterogeneous Metal Nanoparticles Assemblies in Diblock Copolymer Micelles

## III-1. Introduction

Noble metal nanoparticles (NPs), especially those of gold and silver, have been studied intensively owing to their unique properties associated with their localized surface plasmon resonance (LSPR), which are coherent oscillation of the metal electrons in resonance with light of certain frequency [6,7-9-11,55,61-63]. The LSPR is highly sensitive to the size and shape as well as interparticle spacing of the NPs. Recent advances has enabled us to control those parameter to further exploited the LSPR properties of NPs. However, in most cases only a single kind of metal NPs was employed. Nanoparticle assembly composed of two different metal NPs are interesting due to potential unique properties that are absent in their corresponding single metal NPs. It is expected that this kind of arrangement could exhibit not only the combination of the properties related to the presence of two different metal NPs, but also new properties due to a synergy between two metals.

On the other hand, diblock copolymers (BCs) in solution can self-associate into a variety of morphologies with features on the nanometer length scale [37-39]. In solvent selective for one block, micelle formation consist of insoluble core surrounded by a soluble corona is observed. These morphologies enable the precise organization of nanoparticle in specific positions within the micellar structures

[34,43-52]. In this context, we synthesize two different metal nanoparticles, i.e. Au and Ag NPs, in micellar system to precisely localized NPs in different locations as a strategy to induce plasmonic coupling between two different metal NPs. Here, we encapsulate Au NPs modified with Raman active ligand inside polystyrene-block-poly(acrylic acid), PS−PAA micelles. Ag NPs were then synthesized in PAA corona by adding $AgNO_3$ as precursor and hydroquinone, a selective reduction agent. The resulting assembly is consist of Au NP core surrounded by Ag NPs.

It is well-known that the LSPR have contribution to surface-enhanced Raman scattering (SERS) allowing gigantic enhancement of Raman signals of analytes adsorbed on a metal surface, particularly at interparticle junction called “hot spots” [7,12,24,64,65,68]. Hence, the SERS properties of the resulting assembly was characterized using 785 nm laser. Moreover, the LSPR properties are strongly size dependent, thereby we tuned the physical dimension of Au NPs core to observed their effect on SERS intensity. Since heterogeneous metal NPs can amplified the SERS intensity, this assembly may provides a promising pathway for the development of ultrasensitive sensors with low limit of detection.

## III-2. Experimental Section

### III-2.1. Material

Gold (III) chloride trihydrate (HAuCl4, 99.9%), 2-naphtalenthiol (99%), sodium citrate tribasic dehydrate (99%), hydroquinone (99%), and silver nitrate (≥ 99%) were

purchased from Sigma-Aldrich and were used as received. N,N-Dimethylformamide (DMF, 99.8%) was obtained from Junsei. Polystyrene-*block*-poly(acrylic acid), PS−PAA, diblock copolymer was obtained from ATRP Solution Inc. The degree of polymerization of PS and PAA in the PS−PAA copolymers was 198 and 55, respectively, with a polydispersity index of 1.12. Dialysis membrane having molecular weight cut off of 3.5 KDa (Spectra/ Por 7) was purchased from Spectrum Laboratories Inc.

### III-2.2. Procedure

#### III-2.2.1. Synthesis of Gold Nanoparticles

Au NPs were synthesized by citrate reduction method. An aliquot of $HAuCl_4$ solution In a typical process, 500 mL aqueous solution of $HAuCl_4 \cdot 3H_2O$ (0.5 mM) was heated to boiling with vigorous stirring, and 25 mL of sodium citrate solution (0.5 g in 25 mL) was immediately added. The mixture was further boiled for 15 min and then cooled to room temperature.

#### III-2.2.2. Synthesis of Gold Nanoparticles up to 50 nm in diameter

Au NPs up to 50 nm in diameter were synthesized by kinetically controlled seeded growth method. Gold seeds were prepared by adding 1 ml $HAuCl_4 \cdot 3H_2O$ (25 mM) into 150 ml sodium citrate (2.2 mM) at 100°C. Once the synthesis was finished the solution was cooled down until the temperature of the solution reached 90°C and 1 ml of $HAuCl_4 \cdot 3H_2O$ (25 mM) was injected. After 30 min the reaction was finished.

This process was repeated twice. After that, the sample was diluted by extracting 55 ml of sample and adding 53 ml of deionized water and 2 ml of sodium citrate (60 mM). This solution was then used as seed solution and the process was repeated again.

### III-2.2.3. Surface Modification of Gold Nanoparticles

The surfaces of Au NPs were modified by ligand exchange reaction using 2-naphthalenethiol, a hydrophobic ligand. To this end, the as-prepared Au NPs were centrifuged (9000 rpm, 40 min) and then redispersed into N,N-dimethylformamide (DMF). Subsequently, 2-naphthalenethiol (180 μL, 1.0 wt % in DMF) was added to the purified Au NP solution (18 mL), which was further incubated at 60°C for 1 h to complete surface modification.

### III-2.2.4. Encapsulation of Au NPs inside PS-PAA core

PS−PAA micelles containing Au NPs in the core micelles (will be denoted as Au@PS−PAA micelles hereafter) were prepared according to a literature method with slight modification. First, independently prepared DMF solutions of 2-naphthalenethiol-modified Au NPs (4.5 mL) and PS−PAA copolymers (4.5 mL, 0.05 wt % in DMF) were mixed together. Second, deionized water (2 mL) was added to the solution mixture such that the $H_2O$ concentration in the total solution becomes ~18 vol %. Third, the mixture was heated to 110°C for 2 h and then slowly cooled to room temperature. Next, the solution was dialyzed against $H_2O$ to remove DMF and residual reagents. In a typical dialysis process, the mixture solution (28 mL) was

added to a dialysis membrane. After clamping, the dialysis membrane was placed in a large beaker filled with $H_2O$, which was then gently stirred at room temperature. Deionized water was exchanged for each 12 h at least two times.

### III-2.2.5. Synthesis of Heterogeneous Metal Nanoparticle Assemblies

The heterogeneous metal NP assemblies were prepared as follows : Au@PS−PAA in an aqueous solution (2.0 mL) were precipitated at the bottom of Eppendorf tube by centrifugation (9000 rpm, 90 min). Subsequently, the supernatant was cautiously removed by micro-pipette. This removal process was repeated by twice. Next, deionized water was added until the absorbance of PS−PAA micelles with the Au NPs at 535 nm became 1.0 when measured by UV-vis spectroscope with a cuvette having a path length of 1.0 cm. To further synthesize Ag NPs in the PAA corona, an aliquot of an aqueous $AgNO_3$ solution (30 μL, 0.01 M) was added to 2 mL of Au@PS−PAA solution in a quartz cuvette and exposed to UV light (~254 nm) using a conventional UV lamp (6 W, Vilber Lourmat) in a dark container for 3 h at 40°C followed by addition of hydroquinone solution (30 μL, 0.01 M).

## III-2.3. Measurement

UV−Vis absorbance data were recorded on a JASCO V-670 spectrophotometer. Dynamic light scattering (DLS) and zeta-potential measurements were performed on a Zetasizer Nano ZS-90 (Malvern Instruments). Transmission electron microscopy (TEM) images were recorded on a Hitachi H-7500 instrument operating at 80 kV.

Samples for TEM were prepared by placing a drop of mixture solution onto a carbon-coated copper grid and dried at ambient temperature. Raman spectra were collected from sample solution on LSI Dimension-P1 Raman Spectrometer using a red LED laser ($\lambda$ = 785 nm) with an exposure duration of 10 s.

## III-3. Results and Discussion

### III-3.1. Synthesis of Heterogeneous Metal Nanoparticles

In selective solvent PS−PAA diblock copolymers spontaneously self-associate into spherical micelles, which consist of a soluble PAA corona and insoluble PS core. These PS-PAA micelles can be used to incorporate NPs in different location. In this regard, we arrange two different metal NP, Au NPs and Ag NPs, in separate location by employing PS-PAA micellar structure to induce the plasmonic coupling between two different NPs. Here, Au NPs were chosen due to their easier preparation and the uniformity of particle size. While Ag NPs are superior in term of the plasmonic efficiency. The schematic of Figure 11 presents the overview of our system that will be discussed throughout this study.

As discussed in previous chapter, PS−PAA micelles contain a single Au NP in the core has been successfully prepared (Figure 6). To functionalize the PAA corona, we synthesized Ag NPs in PAA corona by utilizing $AgNO_3$ and hydroquinone as described in the experimental section. Hydroquinone (HQ) is a selective reduction agent which has unique properties where it only able to reduce silver ions in the

presence of pre-formed seed particles [72-74]. The UV-Vis spectra of unseeded solution in Figure 12a shows that if HQ is added into an aqueous solution of $AgNO_3$ without PS−PAA micelles, it is unable to react with silver ions on its own, there is no change in the plasmon peak (blue line). Therefore, we employed photoreduction strategies by exposing the micellar solution to UV light having a wavelength of 254 nm in attempt to generate silver seeds. Here, an aqueous $AgNO_3$ (10 mM) solution was added to the micellar solution followed by UV irradiation for 3 h. In this circumstance, the carboxylate anions in the PAA block will coordinate with $Ag^+$ ions to generate silver seeds. A new extinction peak of Ag NPs appears at ~410 nm, which indicates the formation of Ag NPs as depicted in blue line (Figure 12b). Subsequently, HQ (10 mM) was added into the mixture contained seed particles and the reaction rate increases significantly, as confirmed by further increase of extinction peak at ~410 nm (green line in Figure 12b). The system was then held for several hours until the extinction peak saturated, which implies the complete reaction of $Ag^+$. The absorbance value of the final assembly typically saturated after overnight. It needs to be noted that the absorbance of Ag NPs has a tail on the longer wavelength side, which overlaps the absorbance of Au NPs. Hence, the growth of Ag NPs leads to the gradual increase in both Ag and Au peaks in the UV spectrum. In addition, the peak position of Ag NPs and Au NPs remain the same through out the reactions. Thus indicates that plasmon hybridization phenomena, which can be observed by spectral shift in the extinction, is certainly not found and the two heterogeneous NPs in the assembly do not interact because an NP−NP interaction.

The formation of a heterogeneous NP assembly in the PS-PAA micelle was further confirmed by TEM and SEM analysis. TEM image in Figure 12c showed that the two different NPs did not grow in the same location. A single Au NP is located in the center of micelle and surrounded by small-sized Ag NPs in the PAA corona. Similar structure also observed from SEM image (Figure 12d), in which Ag NPs form uniform shell surrounding the Au NP. It needs to be noted that the core and corona structures are not distinguishable in the TEM and SEM images because of the low contrast between PS and PAA blocks. However, from the molecular weight composition, it is reasonable to consider that PS-PAA micelles in this study form crew-cut micelles consisting of a bulky PS core with a thin PAA corona.

Based on this information, we considered that the unchanged extinction peaks in the Figure 12b can be attributed to this separation of the Au NP and Ag NPs in the micellar structures. Moreover, it also implies that Ag NPs mostly get larger on the corona region. If Ag NPs were allowed to grow toward the core, it will induce a Au-Ag coupling effect, resulting in a spectral shift. However, in this experiments, a spectral change was not observed in the UV-Vis spectra. Hence, the heterogeneous NP assemblies with micellar structure in Figure 12c will be denoted as Au@PS−PAA@Ag hereafter.

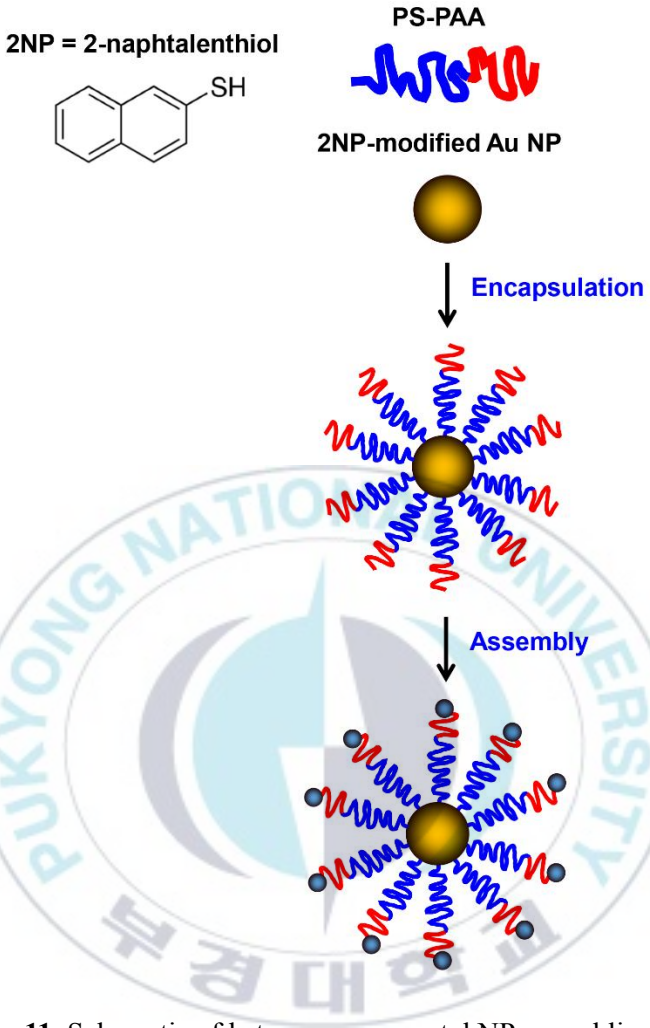


**Figure 11.** Schematic of heterogeneous metal NP assemblies.

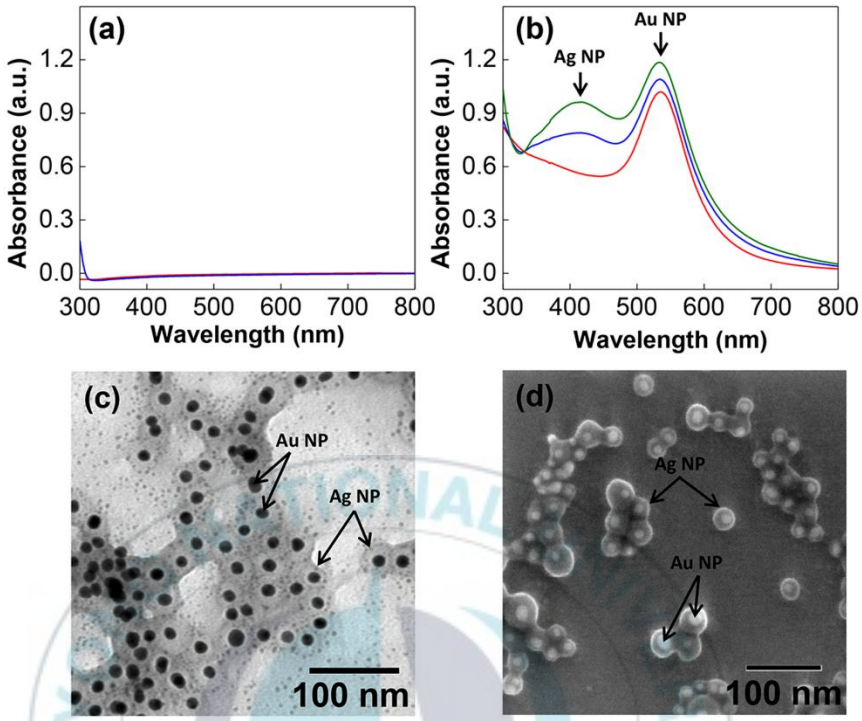


**Figure 12.** (a,b) UV–Vis spectra of (a) $AgNO_3$ solution upon UV irradiation (red) and added hydroquinone (blue) (b) Au@PS−PAA micelles (red) Au@PS−PAA@Ag micelles after UV irradiation (blue) and added hydroquinone (green) (c) TEM image of Au@PS−PAA@Ag micelles (d) SEM image of Au@PS−PAA@Ag micelles.

## III-3.2. Surface-Enhanced Raman Scattering (SERS) Properties of Heterogeneous Metal Nanoparticles

Metal nanoparticles have been well known to amplify Raman signal of analytes that are in a certain proximity of the metal surface due to the large electromagnetic field induced by LSPR. In this context, we attempted to measure the SERS activity of the heterogeneous metal NP assembly by exposing the reaction mixtures containing Au@PS−PAA@Ag micelles to 785 nm diode laser. Note, the core particles in this assemblies were modified by Raman active ligand, 2-napthalenthiol (2-NP). Herein, the 2-NP were selected because its Raman spectra are well-known [68-70].

The characteristic Raman spectra of Au@PS−PAA@Ag assemblies can be seen in Figure 13. For comparison purpose, the SERS activity of Au@PS−PAA micelles were also observed, the result of which is depicted in red line. The SERS intensity increase as we introduce Ag NPs into the micellar hybrid system (blue line in Figure 13). Thus, the dramatically different intensity of Raman signal detected is result from pairs of directly adjacent metal NPs. The gap between heterogeneous metal NPs contains 'hot spots' or region of intense electromagnetic fields that give rise to the enormous enhancement of SERS activity. Raman-active ligand trapped in these hot spots generate SERS signals when illuminate with light exciting the hot spots. Moreover, SERS spectra obtained from this assembly display most prominent Raman signals at 1067, 1381, 1580 and 1622 $cm^{-1}$, which correspond to the C−H bend and ring stretch vibrations of 2-NP, respectively (Figure 13).

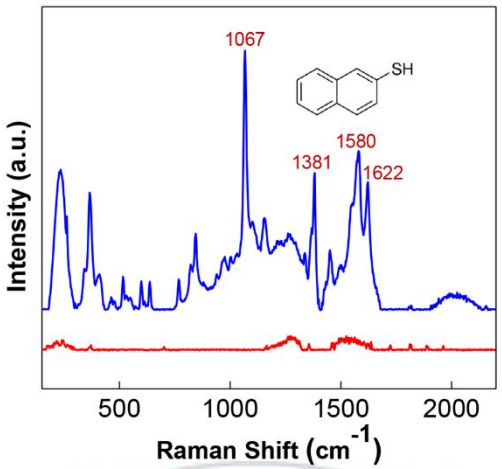


**Figure 13.** Raman spectra of Au@PS−PAA micelles (red) and Au@PS−PAA@Ag micelles (blue) excited with 785 nm laser lines.

To investigate the growth of Ag NPs in the micellar hybrid and the SERS activity more closely, UV-Vis and Raman spectra were obtained at different period of HQ reaction from two independent mixture solution. As evidence from Figure 14a-b, it is found that the plasmon extinction peak at ~410 nm increased as more $Ag^{+}$ was reduced, which results in the intense SERS signals. The above observations further verified that in presence of Ag NPs the SERS activity of the assembly is greatly amplified.

In addition, we have employed the most intense peak at 1067 $cm^{-1}$ to investigate the growth of SERS intensity by plotting the SERS intensity as a function of time (Figure 14c). For instance, after 30 min of HQ addition, the SERS signal of Au@PS−PAA@Ag assemblies was greatly increased. This value was further increase with the reaction time.

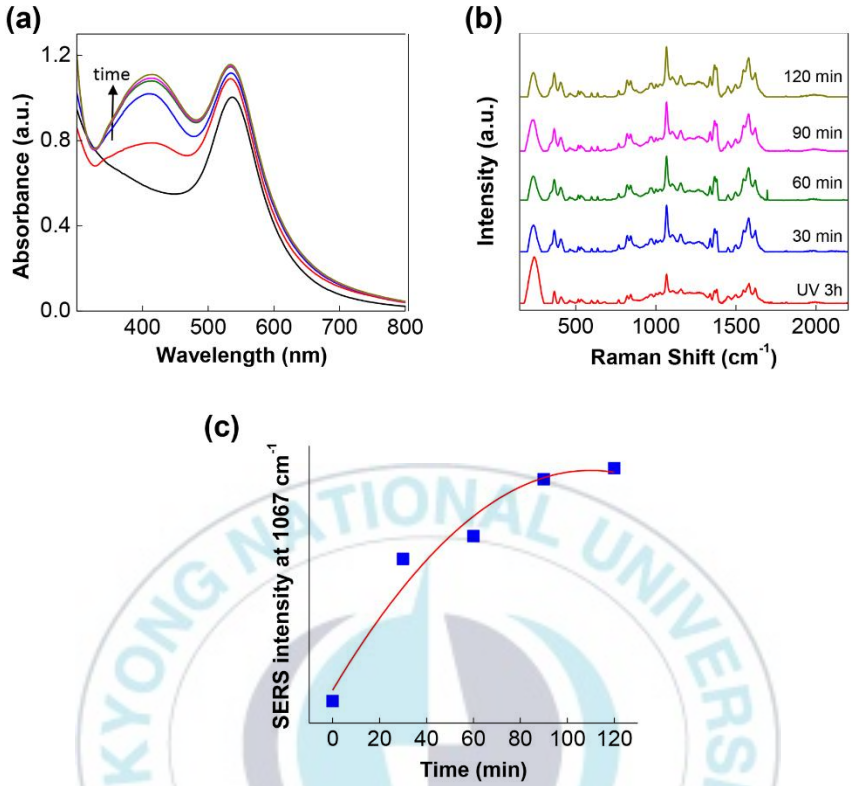


**Figure 14.** (a,b) Time-dependent (a) UV-Vis spectra of Au@PS−PAA@Ag micelles (b) Raman spectra of Au@PS−PAA@Ag micelles (c) Plot of time-dependent SERS intensity at 1067 $cm^{-1}$

### III-3.3. Core Size Effect

It has been shown that the LSPR could be altered by changing the physical dimension of NPs [6,7-9-11,55,61-63]. In typical case, the initial Au NPs used were 12.0 nm in diameter. Hence, we grew Au NPs having distinct size differences using kinetically controlled seeded growth method to examine how physical dimension of Au NP core affects the heterogeneous metal NPs properties. The dynamic light scattering results and TEM images of Au NPs with different particle size are depicted in Figure 15. DLS result shows that the particles synthesized presented excellent morphology and narrow size distributions. As shown in TEM image, the particle size of the Au NPs increased from 26.0 nm to 40.0 nm and 50.0 nm after different growth step.

At this point, the resultant Au NPs were used as core for Ag NPs synthesize. The Ag NPs prepared as describes in experimental section.

Evidence of the formation of Au@PS−PAA@Ag assemblies can be seen from the UV-Vis data (Figure 16). Here, an increase in plasmon band at ~410 nm attributes to Ag NPs after $AgNO_3$ and HQ added can be observed. The final morphology of the assemblies were further confirmed by TEM analysis (Figure 16), where it shows that the synthesized Ag NPs were located in the PAA region of the micellar structure.

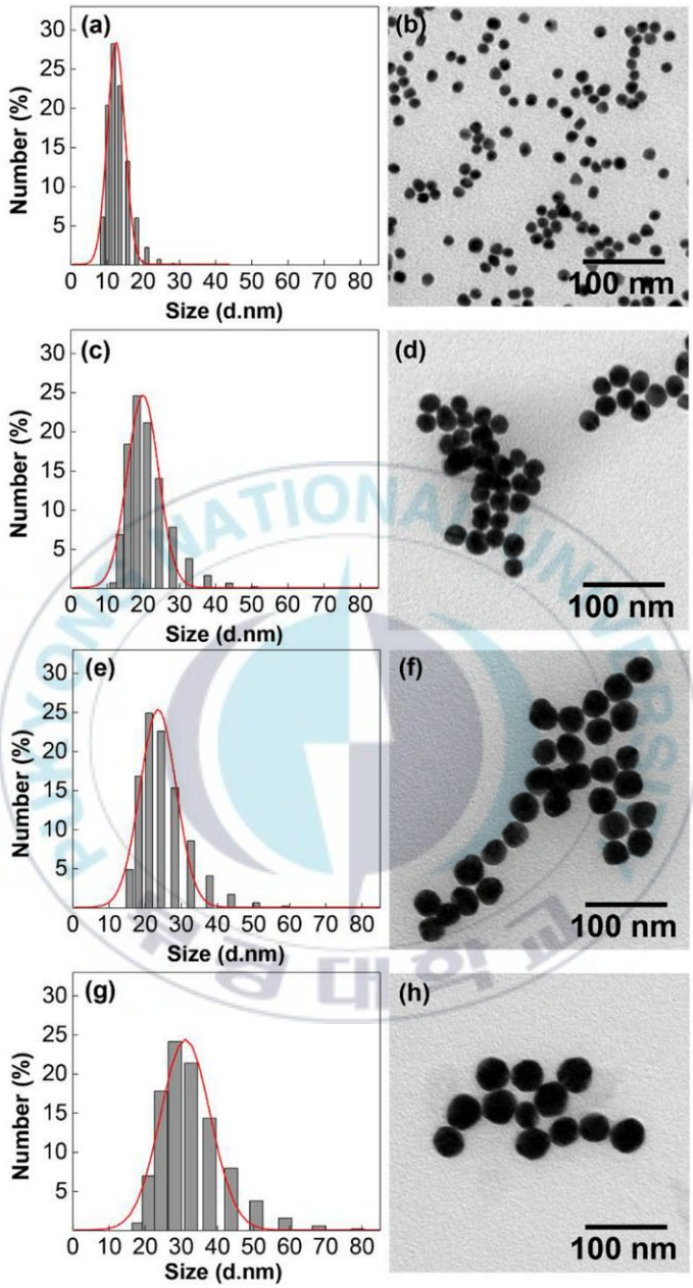


**Figure 15.** DLS results and TEM images of Au NPs having different size : (a,b) 12 nm, (c,d) 26 nm (e,f) 40 nm (g,h) 50 nm.

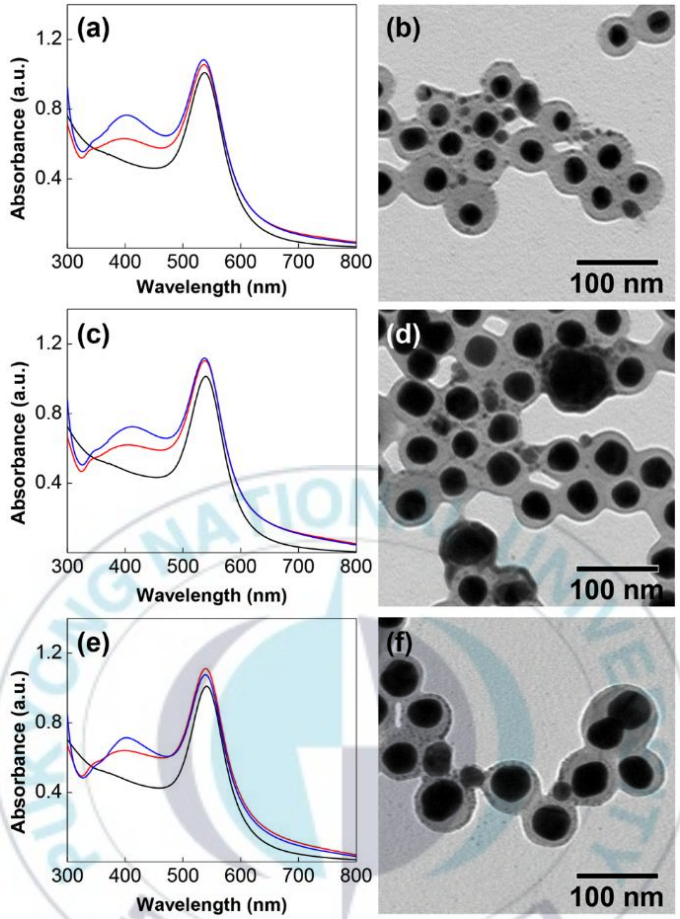


**Figure 16.** UV-Vis spectra and TEM images of heterogeneous metal NP with different Au NP core size : (a,b) 12 nm, (c,d) 26 nm (e,f) 40 nm (g,h) 50 nm.

Next, we focus our attention toward the SERS properties of the heterogeneous metal NP assemblies with different Au core size. The SERS activity of heterogeneous metal NPs was evaluated by calibrating the concentration of the micellar hybrid solution using the equation reported by Liu and coworkers [75]. Where ε is extinction coefficient in $M^{-1}cm^{-1}$, $D$ is the core diameter of the NPs, $k$ = 3.32111, and $a$ = 10.80505.

$$\ln \varepsilon = k \ln D + a$$

Subsequently we calculate the absorbance of the mixture according to Lambert-Beer law, where $A$ is absorbance, ε is extinction coefficient in $M^{-1}cm^{-1}$, $b$ is path length of the beam of light through the nanoparticle solution in cm, and $C$ is molar concentration of nanoparticle solution in mol $L^{-1}$.

$$A = \varepsilon b C$$

The SERS response from the assemblies were plotted in Figure 17. It is assumed that all NPs in the assemblies contribute to the observed SERS signals. Furthermore, it shows a consistent increase in the signal intensity, due to the increase of physical dimension of Au NPs in the core from 12 nm (black line) to 26 nm (red line) to 40 nm (blue line) and 50 nm (green line).

Thus, one can conclude that increase in the size of the Au NPs leads to an increase in

the SERS intensity and in order to improve SERS sensitivity one has to use large Au NPs because the ability of Au NPs to amplify SERS signal is size-dependent.

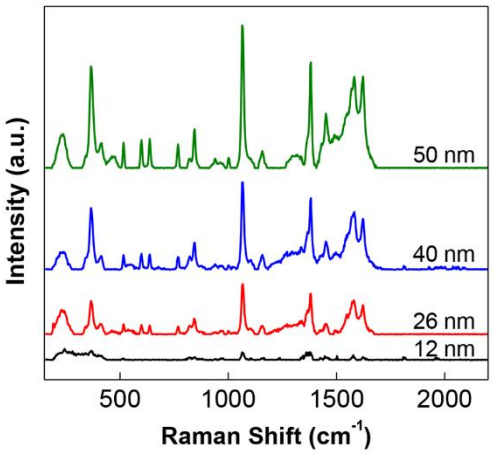


**Figure 17.** Raman spectra of heterogeneous metal NP with different Au NP core size after calibrated. Each color represents different core size : (black) 12 nm, (red) 26 nm, (blue) 40 nm, (green) 50 nm.

### III-3.4. SERS Enhancement Factor

Estimation of the experimental enhancement factors is important for characterizing the SERS effect. The SERS enhancement factor (EF) ratio is calculated for a selected vibrational frequency (1067 $cm^{-1}$).

Assuming that the orientation of Raman active ligand (2-NP) are parallel to the surface of Au NP, we calculate the analytical enhancement factor of the heterogeneous metal NP assemblies under identical experimental conditions using the following equation [76].

$$\mathrm{EF} = \frac{I_{SERS}/c_{SERS}}{I_{RS}/c_{RS}}$$

Where $I_{SERS}$ is SERS signal from the Au@PS−PAA@Ag sample, $c_{SERS}$ is the concentration of the 2-NP on the gold surface, $I_{RS}$ denote Raman spectral intensities under non-SERS conditions, $c_{RS}$ is concentration of 2-NP. Summary of the calculation of the analytical enhancement factor was showed in Table 1.

**Table 1.** Summary of the analytical enhancement factor

| Core size, $D$ (nm) | $I_{SERS}/c_{SERS}$ | $I_{RS}/c_{RS}$ | EF |
|---|---|---|---|
| **12** | 9.66 x $10^8$ | 6.23 x $10^3$ | 1.55 x $10^5$ |
| **26** | 1.56 x $10^9$ | 6.23 x $10^3$ | 2.50 x $10^5$ |
| **40** | 1.14 x $10^9$ | 6.23 x $10^3$ | 1.83 x $10^5$ |
| **50** | 1.18 x $10^9$ | 6.23 x $10^3$ | 1.89 x $10^5$ |

Our measured and calculated maximum enhancement factors are of the order of $10^4$. These results suggest the gap plasmon in the NP assembly contribute significantly to the observed enhancement. However, this range is somewhat smaller than that generally quoted for SERS, $10^6$-$10^8$. There may be several reasons for this difference. For instance, it was observed that there is a fine partitioning between Au and Ag NPs in the micellar structure, which inhibited the interaction between the two different metal NPs. Hence, it is possible to increase the enhancement factor by reducing the distance between Au and Ag NPs in the assembled structure for the future development.

## III-4. Conclusion

In this study, we have demonstrated a strategy for arranging heterogeneous metal nanoparticles in micellar structure. The self-segregating properties of PS−PAA micelles enabled the nanoscale arrangement of heterogeneous metal NPs, in which Au NP in the core is surrounded by Ag NPs in the corona. In addition, we prepared the heterogeneous metal NP assembly with different core sizes. Since metal NPs have

been well known to enhance Raman signal of analytes attached on their surface, we further investigate the SERS property of the heterogeneous metal NP assembly. As a result, the produces assemblies shows greatly enhanced SERS activity compare to their corresponding single metal NPs. The SERS properties of assembly can be tuned by simply changing the core Au NP size. The SERS intensity gradually increased with increasing Au NP sizes. Based on this results, the heterogeneous metal NP can be further developed as a way to improve the detection limit of the sensors.

# References


[1] K. L. Kelly, E. Coronado, L. L. Zhao and G. C. Schatz (2003), *J. Phys. Chem. B.*, **107**, 668.

[2] Y. Xia, Y. Xiong, B. Lim and S. E. Skrabalak (2009), *Angew. Chem. Int. Ed.,* **48**, 60.

[3] M. C. Daniel and D. Astruc (2004), *Chem. Rev.*, **104**, 293.

[4] S. Eustis and M. A. El-Sayed (2006), *Chem. Soc. Rev.*, **35**, 209.

[5] M. A. El-Sayed (2001), *Acc. Chem. Res.*, **34**, 257.

[6] K. A. Willets and R. P. Van Duyne (2007), *Annu. Rev. Phys. Chem.*, **58**, 267.

[7] G. Baffou and R. Quidant (2014), *Chem, Soc. Rev.*, **43**, 3898.

[8] P. K. Jain, X. Huang, I. H. El-Sayed and M. A. El-Sayed (2007), *Plasmonic*, **2**, 107.

[9] P. K. Jain, X. Huan and M. A. El-Sayed (2007), *Nano Today*, **2**, 18.

[10] A. O. Govorov and H. H. Richardson (2007), *Nano Today*, **2**, 30.

[11] E. A. Coronado, E. R. Encina and F. D. Stefani (2011), *Nanoscale*, **3**, 4042.

[12] T. Chen, H. Wang, G. Chen, Y. Wang, Y. Feng, W. S. Teo, T. Wu and H. Chen (2010), *ACS Nano*, **4**, 3087.

[13] E. Smith and G. Dent (2005), "Modern Raman Spectroscopy – A Practical Approach", John Wiley & Sons, Ltd, England.

[14] M. Fleischmann, P. J. Hendra and A. J. McQuillan (1974), *Chem. Phys. Lett.*, **26**, 163.

[15] M. Moskovits (2005), *J. Raman Spectrosc.,* **36**, 485.

[16] A. K. Samal, L. Polavarapu, S. Rodal-Cedeira, L.M. Liz-Marzán, J. Pérez-Juste and I. Pastoriza-Santos (2013), *Langmuir*, **29**, 15076.

[17] M. Moskovits (1985), *Rev. Mod. Phys.,* **57**, 783.

[18] X. Qian, X. Peng, D. O. Ansari, Q. Yin-Goen, G. Z. Chen, D. M. Shin, L. Yang, A. N. Young, M. D. Wang, and S. Nie (2008), *Nat. Biotechnol.*, **26**, 83.

[19] Y. Yang, J. Liu, Z. Fu and D. Qin (2014), *J. Am. Chem. Soc.,* **136**, 8153.

[20] Y. Feng, Y. Wang, X. Song, S. Xing and H. Chen (2016), *Chem. Sci.,* **8**, 430.

[21] F. L. Yap, P. Thoniyot, S. Krishnan and S. Krishnamoorthy (2012), *ACS Nano*, **6**, 2056.

[22] T. Y. Olson, A, M. Schwatzberg, C. A. Orme, C. E. Talley, B. O'Connell and J. Z. Zhang (2008), *J. Phys. Chem.,* **112**, 6319.

[23] S. J. Lee, A. R. Morrill and M. Moskovits (2006), *JACS*, **128**, 2200.

[24] G. Chen, Y. Wang, M. Yang, J. Xu, S. J. Goh, M. Pan and H. Chen (2010), *J. Am. Chem. Soc.,* **132**, 3644.

[25] F. S. Bates (1990), *Annu. Rev. Phys.Chem*, **41**, 525.

[26] M. W. Matsen and F. S. Bates (1995), *Macromolecules*, **29**, 1091.

[27] J. M. G. Swann and P. D. Topham (2010), *Polymers*, **2**, 454.

[28] Y. Mai and A. Eisenberg (2012), *Chem. Soc. Rev.,* **41**, 5969.

[29] Y. Kang and T. A. Taton (2005), *Angew. Chem. Int, Ed.,* **44**, 409.

[30] Y. Mai and A. Eisenberg (2012), *Acc. Chem. Res*, **45**, 1657.

[31] A. Sánchez-Iglesias, M. Grzelczak, T. Altantzis, B. Goris, J. Pérez-Juste, S. Bals, G. V. Tendeloo, S. H. Donaldson Jr., B. F. Chmelka, J. N. Israelachvili and L. M. Liz-Marzán (2012), *ACS Nano*, **6**, 11059.

[32] G. Schneider and G. Decher (2004), *Nano Lett.*, **4**, 1833.

[33] G. Schneider and G. Decher (2006), *Nano Lett.*, **6**, 530.

[34] S. H. Jo, H. W. Kim, M. Song, N. J. Je, S. Oh, B. Chang, J. Yoon, J. H. Kim, B. Chung and S. I. Yoo (2015), *ACS Appl. Mater. Interfaces*, **7**, 18778.

[35] S. H. Kim, K. Kim, K. Char, S. I. Yoo and B. Y Sohn (2016), *Nanoscale*, **8**, 10823.

[36] J. H. Kim, M. Zakia, J. H. Kim, S. S. Park, J. Yoon, P. Huh and S. I. Yoo (2017), *J. Appl. Poly. Sci.,* **133**, 44693.

[37] M. Moffitt, K. Khougaz and A. Eisenberg (1996), *Acc. Chem. Res*, **29**, 95.

[38] S. Förster and T. Plantenberg (2002), *Angew. Chem. Int. Ed.,* **41**, 688.

[39] I. W. Hamley (1988), "The Physics of Block Copolymers", Oxford University Press, New York.

[40] J. Wang, W. Li and J. Zhu (2014), *Polymers*, **55**, 1079.

[41] Y. Liu and X. Wang (2011), *Polym. Chem.*, **2**, 2741.

[42] Y. Kang and T.A. Taton (2005), *Macromolecules.,* **38**, 6115.

[43] Q. Luo, R. J. Hickey, and S. Park (2013), *ACS Macro Lett.*, **2**, 107.

[44] T. Chen, M. Yang, X. Wang, L. H. Tan and H. Chen (2008), *J. Am. Chem. Soc.,* **130**, 11858.

[45] H. W. Kim, J.W. Kim, S. H Jo, C. Lee, W. Lee, S. S. Park, B. Chung and S. I. Yoo (2015), *Soft Matter*, **11**, 4402.

[46] K. Kim, J. H. Kim, K. Kim, F. Laquai, E. Arifin, J. Lee, S. I. Yoo and B. H Sohn (2012), *ACS Nano*, **6**, 5051.

[47] N. Nasongkla, E. Bey, J. Ren, H. Ai, C. Khemtong, J. S. Guthi, S. Chin, A. D. Sherry, D. A. Boothman, J. Gao (2006), *Nano Lett.,***6**, 242717.

[48] M. Yang, G. Chen, Y. Zhao, G. Silber, Y. Wang, S. Xing, Y. Han and H. Chen (2010), *Phys. Chem. Chem. Phys.,***12**, 11850.

[49] J. He, X. Huang, Y. Li, Y. Liu, T. Babu, M. A. Aronova, S. Wang, Z. Lu, X. Chen and Z. Nie (2013), *J. Am. Chem. Soc.,* **135**, 7974.

[50] A. S. Urban, X. Shen, Y. Wang, N. Large, H. Wang, M. W. Knight, P. Nordlander, H. Chen and N. J. Halas (2013), *Nano Lett.,* **13**, 4399.

[51] H. Wang, L. Chen, X. Shen, L. Zhu, J. He and H. Chen (2012), *Angew. Chem. Int. Ed.,* **124**, 8145.

[52] Y. Guo, S. Harirchian-Saei, C. M. S. Izumi and M. Moffitt (2011), *ACS Nano*, **5**, 3309.

[53] L. Zhang, K. Yu and A. Eisenberg (1996), *Science*, **272**, 1777.

[54] L. Zhang and A. Eisenberg (1996), *Macromolecules*, **29**, 8805.

[55] S. Sheikholeslami, Y. Jun, P. K. Jain and A.P. Alivisatos (2010), *Nano Lett.,***10**, 2655.

[56] P. K. Jain, W. Huang and M. A. El-Sayed (2007), *Nano Lett.,* **7**, 2080.

[57] R. Hariharan, C. Biver, J. Mays, W. B. Russel (1998), *Macromolecules*, **31**, 7506.

[58] J. Li, K. D. Caldwell and N. Rapoport (1994), *Langmuir*, **10**, 4475.

[59] S. I. Yoo and B.H. Sohn (2016), *Macromol. Res.,* **24**, 292.

[60] J. G. Son, A. F. Hannon, K. W. Gotrik, A. Alexander-Katz and C. A. Ross (2011), *Adv. Mater.*, **23**, 634.

[61] W. Rechberger, A, Hohenau, A. Leitner, J. R. Kreen, B. Lamprecht and F. R. Aussenegg (2003), *Opt. Com.,* **220**, 137.

[62] P. K. Jain, K. S. Lee, I. H. El-Sayed and M. A. El-Sayed (2006), *J. Phys. Chem. B.,* **110**, 7238.

[63] S. Link and M. A. El-Sayed (1999), *J. Phys. Chem. B.,* **103**, 8410.

[64] B. Nokoobakht, J. Wang and M. A. El-Sayed (2002), *Chem. Phys. Lett.,* **366**, 17.

[65] F. L. Yap, P. Thoniyot, S. Krishnan and S. Krishnamoorthy (2012), *ACS Nano,* **6**, 2056.

[66] J. P. Camden, J. A. Dieringer, J. Zhao and R. P. V. Duyne (2008), *Acc. Chem. Res.,* **41**, 1653.

[67] P. Pinkhasova, L. Yang, Y. Zhang, S. Sukhishvili and H. Du (2012), *Langmuir,* **28**, 2529.

[68] R. A. Alvarez-Puebla, D. J. Ross, G. A. Nazri and R. F. Aroca (2005), *Langmuir,* **21**, 10504.

[69] R. A. Alvarez-Puebla, D. S. D. Santos Jr. and R. F. Aroca (2004), *Analyst,* **129**, 1251.

[70] N. Pazos-Perez, F. J. Garcia de Abajo, A. Fery and R. A. Alvarez-Puebla (2012), *Langmuir,* **28**, 8909.

[71] N. L. Rosi and C. A. Mirkin (2005), *Chem. Rev.,* **105**, 1547.

[72] M. A. Pérez, R. Moiraghi, E. A. Coronado and V. A. Macagno (2008), *Cryst. Growth Des.,* **8**, 1377.

[73] S. T. Gentry, S. J. Fredericks and R. Krchnavek (2009), *Langmuir,* **25**, 2613.

[74] S. T. Gentry and S. D. Levit (2009), *J. Phys. Chem. C.,* **113**, 12007.

[75] X. Liu, M. Atwater, J. Wang and Q. Huo (2007), *Colloids Surf. B.,* **58**, 3.

[76] E. C. L. Ru, E. Blackie, M. Meyer and P. G. Etchegoin (2007), *J. Phys. Chem,* **111**, 13794.

# Acknowledgements

First and foremost I would like to thank my advisor, Professor Seong Il Yoo, for the help and support. I have learned so much and would not be where I am today without your support. Next, I would like to thank my mother and brother for believing in me and supporting me in many different ways to help me achieve my goals. There are not enough words that can thank you for everything you have helped me emotionally and physically. You put no limits on my dreams or anything else I wish to do. Even when I didn't believe in myself, you have always believed in me and what I could achieve.

I would also like to thank the amazing friends that I have made here in Busan. You have been my family away from home and I will always treasure the memories we made here. Finally I would like to thank the members of the Yoo's group, both past and present : Kim Jang Hwan, Je Nam Jin, Song Chang Hyun, Limpat for your help and support.

Pukyong National University, Busan, South Korea

June 2017

Maulida Zakia